Supplementary Information for “Reconstruction of past exposure to natural hazards driven by historical statistics: HANZE v2.0”

Contents

Supplementary Figure S1. HANZE domain

Supplementary Figure S1. HANZE domain. National boundaries outside the study area based on Natural Earth (2022). See Table S1 for sources of boundary data within the study area.

Supplementary Table S1. Sources of administrative boundaries

Supplementary Table S1. Sources of administrative boundaries. Countries not listed here were collected from OpenStreetMap (© OpenStreetMap contributors 2022. Distributed under the Open Data Commons Open Database License (ODbL) v1.0). All links last accessed 5 May 2022.

Country	Provider	Dataset name	URL
Austria	Bundesamt für Eich- und Vermessungswesen	*Verwaltungsgrenzen (VGD) - Stichtagsdaten grundstücksgenau*	[1]
Belgium	FPS Finance - General Administration of Patrimonial Documentation (GAPD)	*Administrative units - Municipalities*	[2]
Estonia	Estonian Administrative and Settlement Division	*Counties*	[3]
Finland	The National Land Survey of Finland	*The regions of Finland 2021 with the 2018 regional codes* [used in combination with OpenStreetMap data]	[4]
Germany	Bundesamt für Kartographie und Geodäsie	*NUTS-Gebiete 1:250 000, Stand 01.01. (NUTS250 01.01.)* [except Mecklenburg-Vorpommern, where OpenStreetMap data were used]	[5]
Greece	Hellenic Mapping and Cadastral Organisation	*Boundaries of Prefectures (HMCO)*; *Boundaries of the Local Authorities (LAs) (pre-Kapodistrian)*	[6][7]
Ireland	Ordnance Survey Ireland	*Small Areas Ungeneralised - OSi National Statistical Boundaries – 2015*; *Local Electoral Areas Boundaries Ungeneralised - OSi National Administrative Boundaries - 2015*	[8][9]
Italy	Istituto Nazionale di Statistica (ISTAT)	*Municipal Boundaries of Italy 2019* [only for Sardegna, otherwise OpenStreetMap provinces used]	[10]
Norway	Kartverket	*Administrative enheter kommuner*	[11]
Poland	Główny Urząd Geodezji i Kartografii	*PRG – jednostki administracyjne*	[12]
United Kingdom	Office for National Statistics	*Local Authority Districts (May 2020) Boundaries UK BFE*	[13]

[1] https://www.data.gv.at/katalog/dataset/verwaltungsgrenzen-vgd-stichtagsdaten-grundstucksgenau

[2] https://www.geo.be/catalog/details/591e7f88-c443-4659-b8b7-23601d647ee6?l=en

[3] https://geoportaal.maaamet.ee/eng/Spatial-Data/Administrative-and-Settlement-Division-p312.html

[4] https://www.avoindata.fi/data/en_GB/dataset/suomen-maakunnat-2021-vuoden-2018-maakuntakoodeilla

[5] https://gdzshopv-lpz.bkg.bund.de/index.php/default/catalog/product/view/id/773/s/nuts-gebiete-1-250-000-stand-01-01-nuts250-01-01/category/8/?___store=default

[6] http://geodata.gov.gr/en/dataset/oria-nomon-okkhe

[7] http://geodata.gov.gr/en/dataset/oria-ota-pro-kapodistria

[8] https://data-osi.opendata.arcgis.com/datasets/small-areas-ungeneralised-osi-national-statistical-boundaries-2015/explore?location=53.424600%2C-8.379100%2C7.63

[9] https://data-osi.opendata.arcgis.com/datasets/1516dc49dfc64395b5a6ff582cba8150_3/explore?location=53.424600%2C-8.379100%2C7.63

[10] https://hub.arcgis.com/datasets/inspire-esri::municipal-boundaries-of-italy-2019/about

[11] https://kartkatalog.geonorge.no/metadata/administrative-enheter-kommuner/041f1e6e-bdbc-4091-b48f-8a5990f3cc5b

[12] https://www.geoportal.gov.pl/dane/panstwowy-rejestr-granic

[13] https://geoportal.statistics.gov.uk/datasets/local-authority-districts-may-2020-boundaries-uk-bfe?geometry=-44.245%2C51.101%2C39.383%2C59.782

Supplementary Figure S2. Regional data availability in HANZE

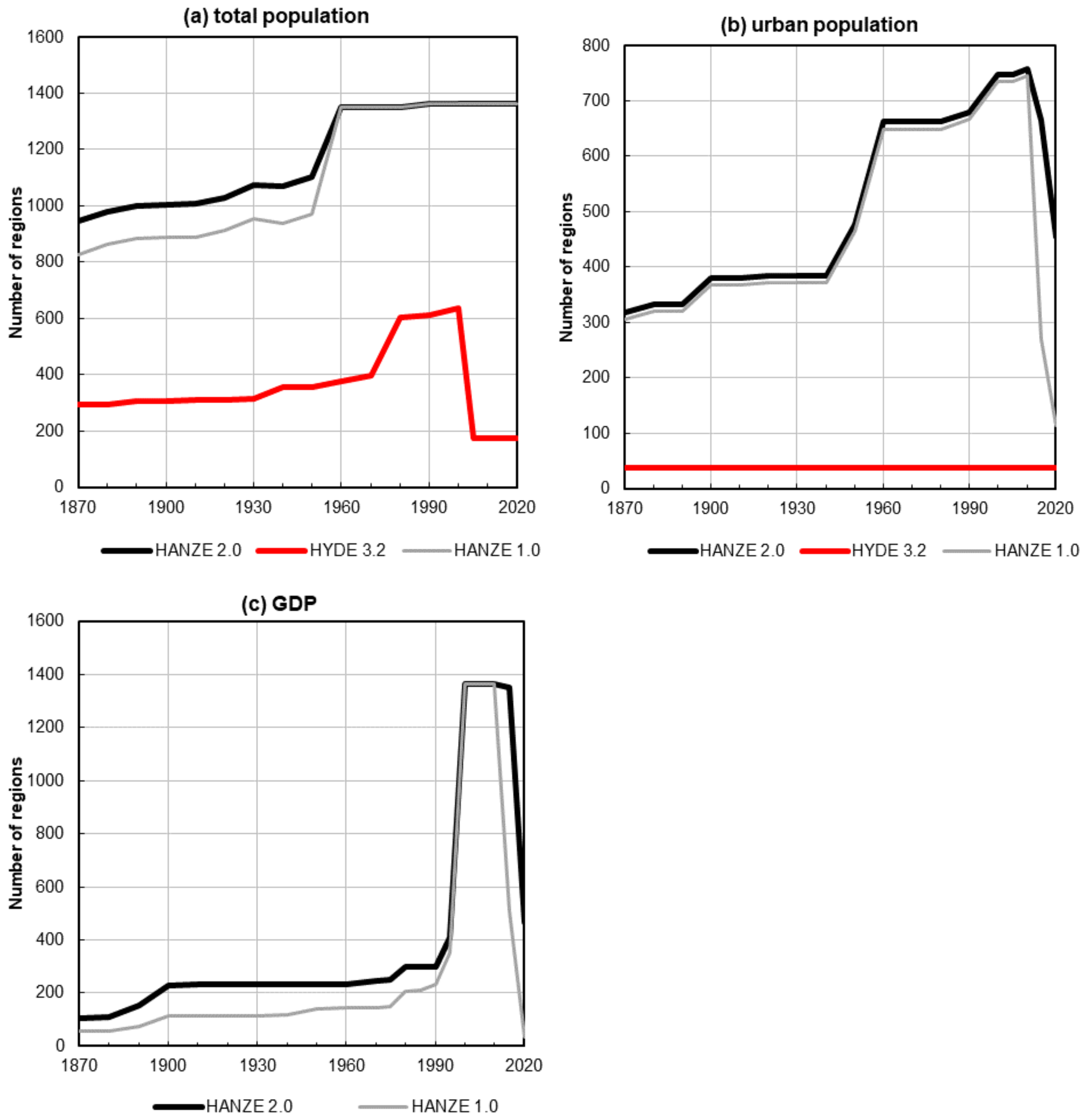

Supplementary Figure S2. Availability of regional data in HANZE (v1 from 2017 and v2 in this study) and HYDE v3.2. The data are for the domain of HANZE v1, i.e. without non-EU Balkan countries, and with a 10-yearly timestep for 1870-2000 and 5-yearly for 2000-2020, except GDP shown with a 10-yearly timestep for 1870-1970 and 5-yearly for 1970-2020.

Supplementary Figure S3. Special case of Dutch land reclamations

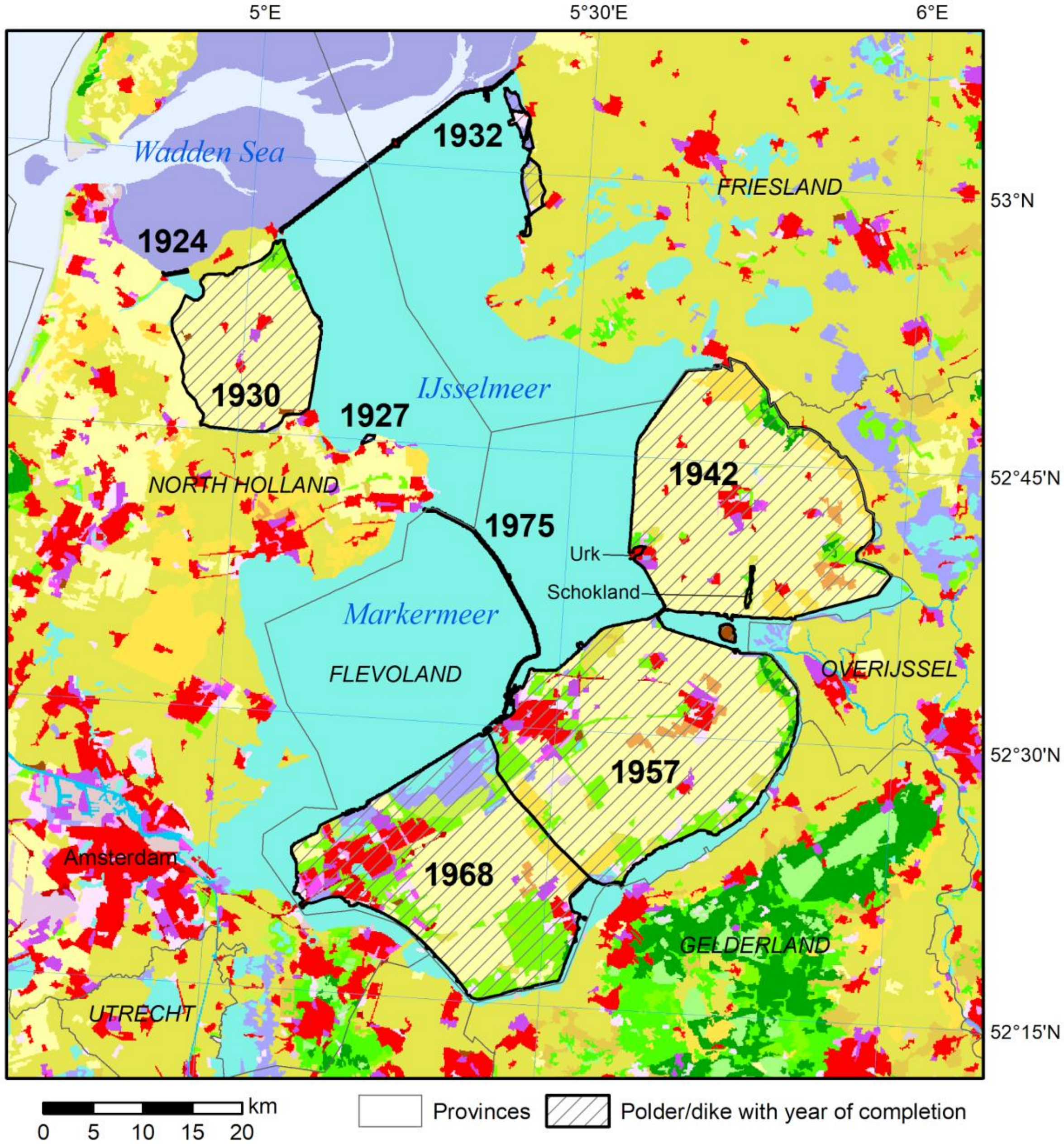

Supplementary Figure S3. „Zuiderzeewerken" land reclamations by year of construction, overlaying Corine Land Cover 2012 map (Copernicus Land Monitoring Service 2022).

Supplementary Text S1. Local population estimates, 1961-2011

Gløersen and Lüer (2013) collected population data at the level of local administrative units (LAUs) based on censuses made from ca. 1960 to 2011. The data were recalculated to a single set of subdivisions to allow consistent comparison through time. For most countries, data represent LAU level 2 (as defined by Eurostat), which is the lowest level of administrative divisions in a given country. For Lithuania and Slovenia, a more aggregated level (LAU 1) was provided. The data was provided at census dates and interpolated (sometimes also extrapolated) to benchmark dates, spanning full decades from 1 January 1961 to 1 January 2011; the interpolated data were used in the analysis. The coverage of the study area is not complete. The following additions were made:

- In North Macedonia, there has been no census since 2002, hence mid-year estimates for 2011 from the Republic of North Macedonia State Statistical Office (2021) was used. Due to gaps in data and spatial data limitations, the population figures were aggregated to LAU 1 level, with 10 LAUs in the Skopje area aggregated further to a single unit;
- Data for Serbia was taken at LAU 1 level from the Statistical Office of the Republic of Serbia (2021);
- For five small countries and territories (Andorra, Isle of Man, Monaco, San Marino, the Vatican), population for the entire territory as compiled in the HANZE database was used.

The Eurostat's dataset doesn't also cover Albania, Bosnia and Herzegovina, Kosovo and Montenegro. Those countries were excluded from further analysis due to difficulty in gathering the necessary population and spatial data. Also, data is completely missing for 240 out of 614 LAUs in Cyprus, however the vast majority of those are located wholly or partially in Northern Cyprus, therefore outside this study's domain. Data is also missing for some years in 15 LAUs located in Czechia (3), Cyprus (1), France (1), Germany (3), Malta (2) and Slovakia (5).

The tabular data were merged with spatial data from Eurostat. As the subdivisions refer to different time points for different countries, and are also not always internally consistent, several datasets produced by EuroGeographics and provided to Eurostat were used ("Communes" for different years and "Census units 2011"). Due to the resolution of spatial data, population figures for Denmark, Greece, North Macedonia and Portugal had to be aggregated to LAU 1 level. For some countries, individual local units had to be aggregated, split or redrawn in order to match the subdivisions used in the population dataset. For 37 out of 3441 LAUs in Ireland and 86 out of 9499 LAUs in the United Kingdom it was to possible to match tabular and spatial data due to large administrative boundary changes.

The final map contains 109,419 LAUs (Fig. S4). Of these, 378 LAUs are not usable due to missing population data and 364 LAUs have no population[1], resulting in a total of 108,679 LAUs with generally consistent population data for 1961-2011. It was noticed for a small number of cases (e.g. for some locations in Italy) that the data were not fully adjusted for administrative boundary changes. Still, the benefit of the dataset for analysing for population changes in Europe is very large.

[1] These are non-municipal areas, e.g. lakes, forests or military bases, occurring in Cyprus, Estonia, France, Germany, Lithuania, North Macedonia, Spain and Switzerland.

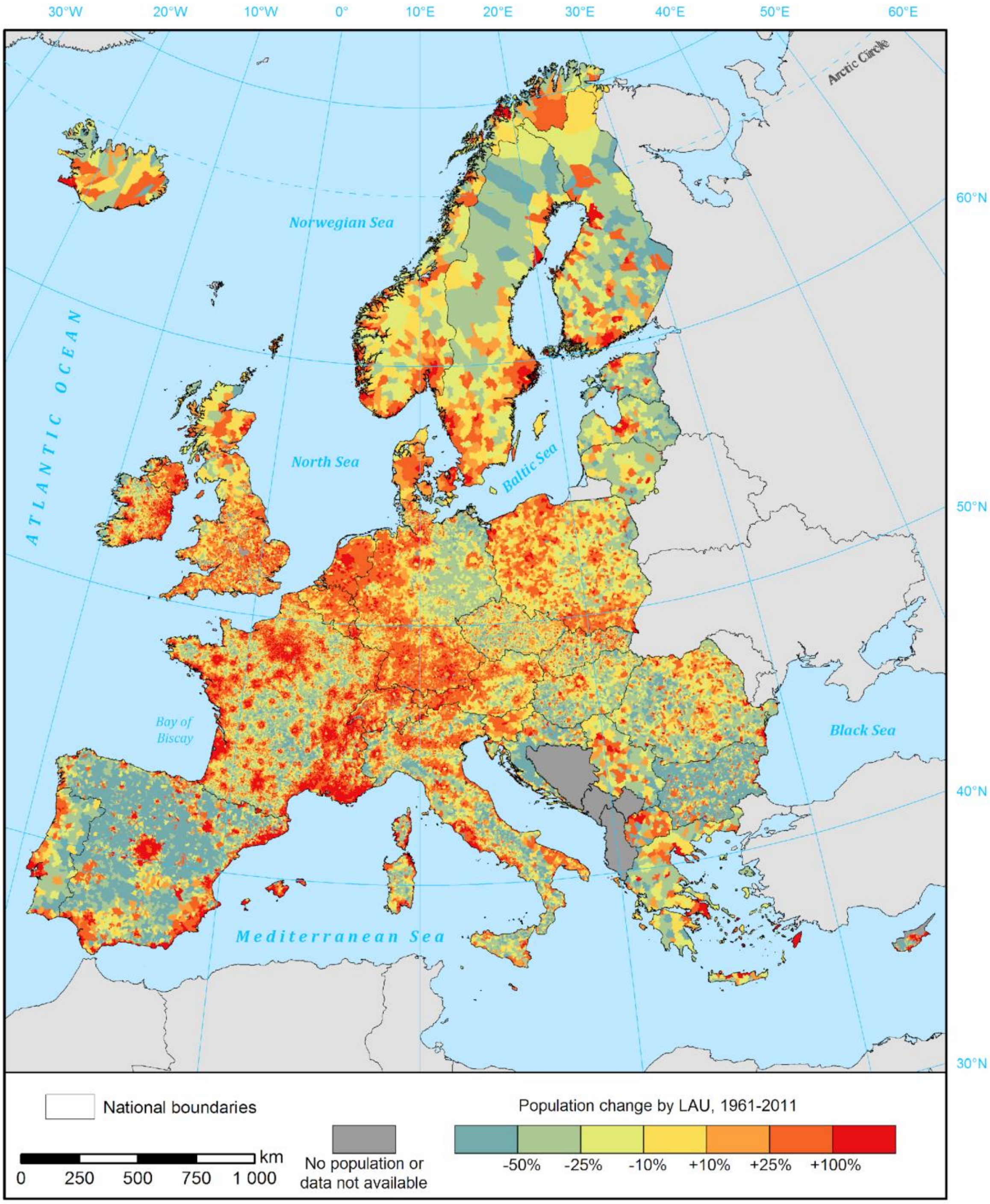

Supplementary Figure S4. Population change by local administrative unit between 1961 and 2011 (see text for data sources). **National boundaries outside the study area based on Natural Earth (2022).**

Supplementary Figure S5. Virtual LAUs

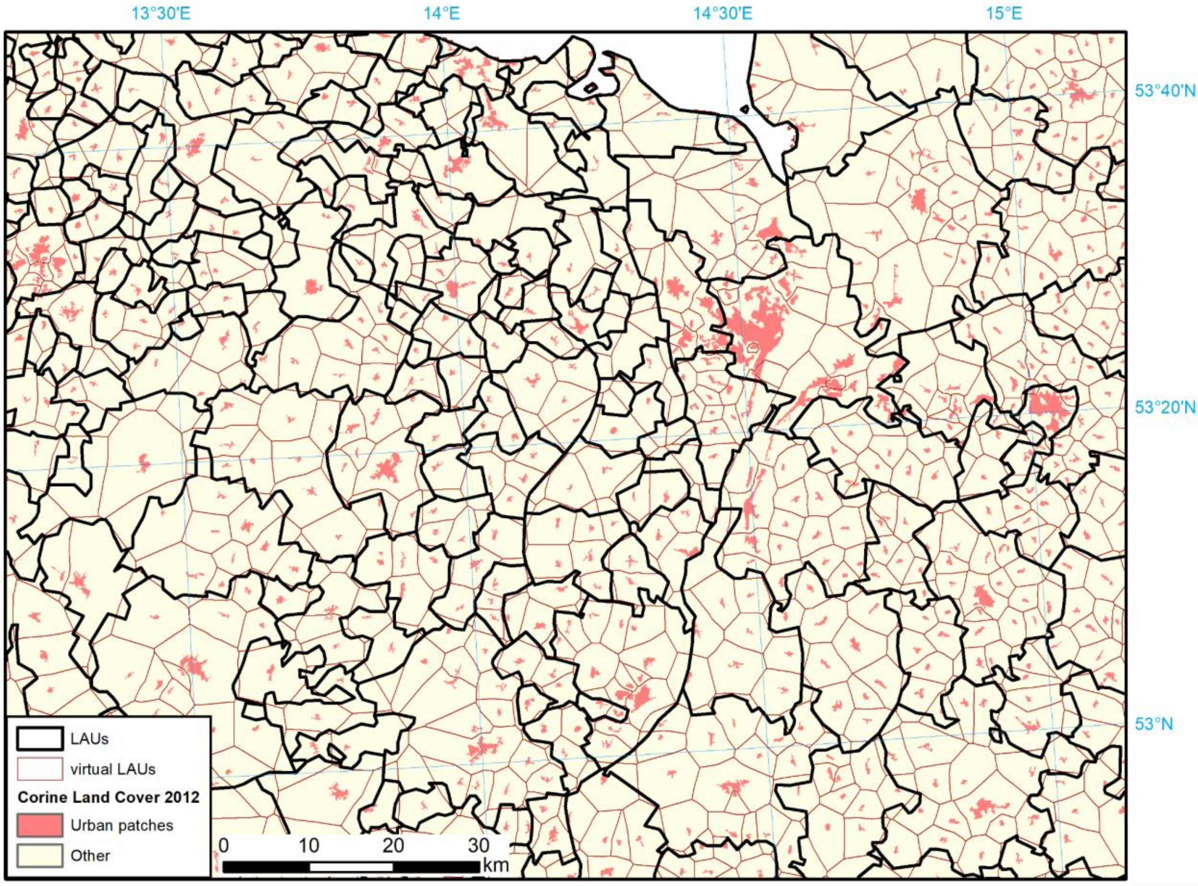

Supplementary Figure S5. Virtual LAUs (red lines) in a fragment of Germany and Poland compared with actual LAUs (black line) from Eurostat 2021.

Supplementary Text S2. Calibrating urban population change

The calibration utilizes Clark's (1951) model of population density, which he described with an exponential function:

$$y = Ae^{-bx} \qquad (1)$$

where y is the population density (in persons per ha), x is the distance from the city centre (in km), A and b are exponential function coefficients. Clark (1951, 1967) provided estimates of A and b for 16 cities in 9 countries for 29 time points. Hourihan (1982) provided additional estimates for 3 cities from several censuses, of which 13 cases were used (estimates made with only a few data points were excluded). That gives a total of 42 estimates spanning a whole century, from 1871 to 1971 (Table S2). In the population map constructed here the population density was calculated for 500 m wide zones around (arbitrarily chosen) city centre, interpolated to match the time points from literature and then fitted to an exponential function. The model was run many times using random weighting of five datasets indicating distance from urban centre. A comparison of function parameters for a most optimal combination is presented in Fig. S6. Overall, the fit is moderate, but a better match of modelled and observed estimates of eq. 1 parameters would be difficult, since the exponential curve fits are very sensitive to the sample size, i.e. spatial resolution of data and maximum distance from the city centre. The latter is not known for all cities. Additionally, the source literature studies used census wards of different sizes instead of a disaggregated population grid used here.

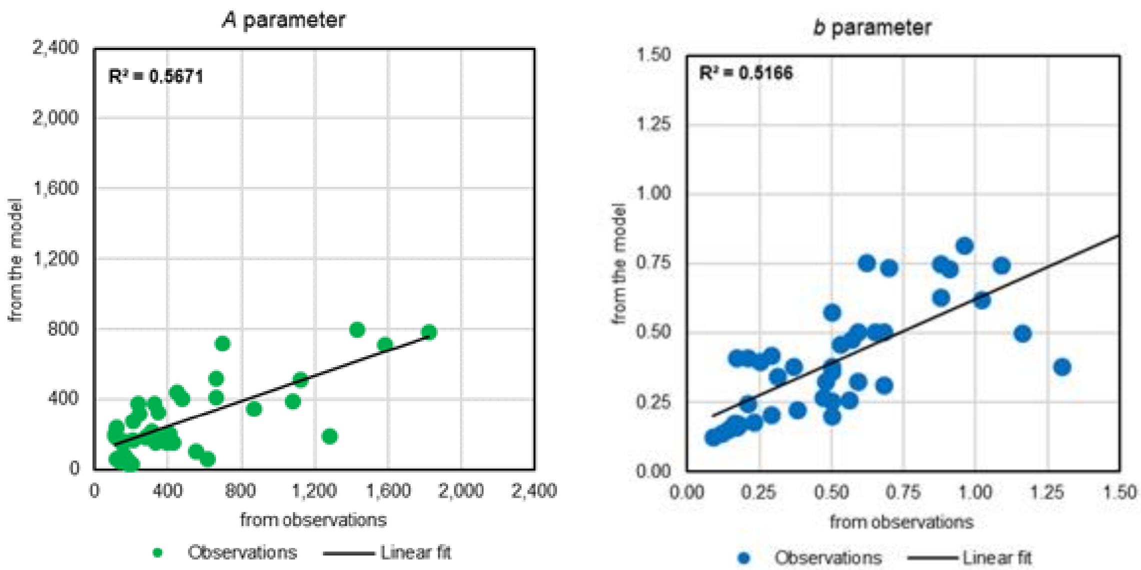

Supplementary Figure S6. Estimates of* A *and* b *parameters (eq. A1) from modelled and observed population data.

Supplementary Table S2. Estimates of urban population density. A, b – exponential function parameters (adjusted to give population density in persons per ha, rather than persons per sq. mile as in Clark 1951 and Hourihan 1982). D – maximum distance from the city centre (km), for which population data were used to calculate exponential function parameters (values in red are estimates, as the source does not specify the distance).

Name	Region	Year	A	b	D	Source
Aarhus	DK042	1950	279	0,96	5	Clark 1967
Berlin	DE300	1885	1120	0,68	8	Clark 1951; Clark 1967
Berlin	DE300	1900	1580	0,59	10	Clark 1951; Clark 1967
Birmingham	UKG31	1921	401	0,50	11	Clark 1967
Birmingham	UKG31	1938	201	0,29	12	Clark 1967
Budapest	HU101	1935	1080	0,56	5	Clark 1951; Clark 1967
Copenhagen	DK011	1940	231	0,37	7	Clark 1967
Cork	IE025	1926	199	1,02	3	Hourihan 1982
Cork	IE025	1936	177	0,88	3	Hourihan 1982
Cork	IE025	1951	176	0,91	4	Hourihan 1982
Cork	IE025	1961	114	0,70	4	Hourihan 1982
Cork	IE025	1971	158	0,62	4	Hourihan 1982
Dublin	IE021	1901	391	0,68	4	Hourihan 1982
Dublin	IE021	1911	379	0,65	4	Hourihan 1982
Dublin	IE021	1926	352	0,59	4	Hourihan 1982
Dublin	IE021	1936	270	0,53	6	Clark 1951; Clark 1967
Dublin	IE021	1951	106	0,25	8	Hourihan 1982
Dublin	IE021	1961	105	0,21	8	Hourihan 1982
Dublin	IE021	1971	113	0,17	8	Hourihan 1982
Frankfurt am Main	DE712	1890	550	1,16	5	Clark 1967
Frankfurt am Main	DE712	1933	340	0,57	6	Clark 1967
Leeds	UKE42	1951	116	0,31	9	Clark 1967
Limerick	IE023	1961	136	1,09	3	Hourihan 1982
Limerick	IE023	1971	126	0,88	3	Hourihan 1982
Liverpool	UKD72	1921	1275	0,50	9	Clark 1951; Clark 1967
London	UKI11	1871	865	0,38	17	Clark 1967
London	UKI11	1901	660	0,23	20	Clark 1967
London	UKI11	1921	443	0,17	25	Clark 1967
London	UKI11	1931	475	0,17	26	Clark 1967
London	UKI11	1939	320	0,14	28	Clark 1967
London	UKI11	1951	240	0,12	29	Clark 1967
London	UKI11	1961	205	0,09	33	Clark 1967
Manchester	UKD31	1931	155	0,16	18	Clark 1951
Manchester	UKD31	1939	143	0,18	20	Clark 1967
Oslo	NO011	1938	308	0,50	4	Clark 1951; Clark 1967
Paris	FR101	1896	1430	0,50	12	Clark 1951; Clark 1967
Paris	FR101	1931	1820	0,47	14	Clark 1951; Clark 1967
Paris	FR101	1946	695	0,21	16	Clark 1967
Stockholm	SE110	1880	610	1,30	10	Clark 1967
Stockholm	SE110	1940	425	0,48	10	Clark 1967
Vienna	AT130	1890	660	0,50	7	Clark 1951; Clark 1967
Zurich	CH040	1936	328	0,29	8	Clark 1967

Supplementary Text S3. Data for the land-use transition model

Data for the land-use transition model, implemented as Bayesian Network, was obtained by sampling the CLC inventory. Firstly, vector layers of CLC-Changes 2000-2006, 2006-2012 and 2012-2018 were obtained (1,194,980 patches). The CLC classes before and after transition were grouped together as follows:

- Urban fabric (CLC 111-112);
- Other artificial (CLC 121-142);
- Croplands (CLC 211-223 and 241-244);
- Pastures (CLC 231);
- Natural (CLC 311-324, 333 and 411-412);
- Other (CLC 331-332, 334-335, 421-523).

CLC-Changes patches transitioning within a given group, or transitioning from/to "Other" classes were excluded from further analysis, leaving 240,870 patches of varying size. To sample the inventory, a "fishnet" of 25x25 km cells was created and clipped to the land mask of the baseline land cover/use map. It was further clipped to the remaining CLC-Changes patches. In each cell of the fishnet, $1+\frac{A}{7}$ samples (rounded to the nearest integer) within the borders of CLC-Changes patches were generated[2], where A is the area of all patches within a fishnet cell (in hectares). The samples were generated at least 100 meters apart due to the resolution of most raster data used throughout this study. In total, 513,915 locations with land-use transitions were obtained. Then, an equal number of samples in each fishnet cell were generated in the remaining area of the cells. In this way, the same number of random locations where no land-use transitions took place between 2000 and 2018 was obtained with the same spatial distribution as the other dataset. Instances of transitions are many times fewer in reality, but as we are interested in the relative probability of transition between CLC classes rather than the total probability, we can sample a greater proportion of transitions to better quantify the patterns of land-use changes. An example of sample locations is presented in Fig. S7.

A smaller validation dataset was created as well. A new set of random points was generated in the fishnet, but the number of samples per cell was capped at 15, resulting in 97,790 samples each for transitions and non-transitions, with a much more even spatial distribution throughout Europe.

The sample locations were used to extract data from various raster datasets, as follows:

- Population density in 2011 computed using kernel density and per "virtual" LAU (see section 3.4.1);
- Euclidean distances from urban centres based on five datasets (see section 3.4.1);
- Elevation (in meters) and slope (per mille) computed from EU-DEM dataset at 100 m resolution (Eurostat 2021);
- Agricultural suitability indices calculated by FAO (2021) in the Global Agro-Ecological Zoning version 4 (GAEZ) database for five different crops (alfalfa, grass, wheat, rye and white potato):
    - Suitability index range (0–10000), with all land in grid cell under rainfed conditions;
    - Output density (potential production divided by total grid cell area) under rainfed conditions;
    - Agro-climatic potential yield with an available water content of 200 mm/m (under irrigation conditions).

[2] Using „Create Random Points" tool in ArcGIS 10.7.1

The agricultural indices were all for the historical period 1971-2000 using CRUTS32 climate data, assuming high input level and without CO_2 fertilization. The indices combine data on climate, soil and terrain to estimate potential yield of various crops. The resolution of this dataset is 5' (about 4–7 km, depending on location).

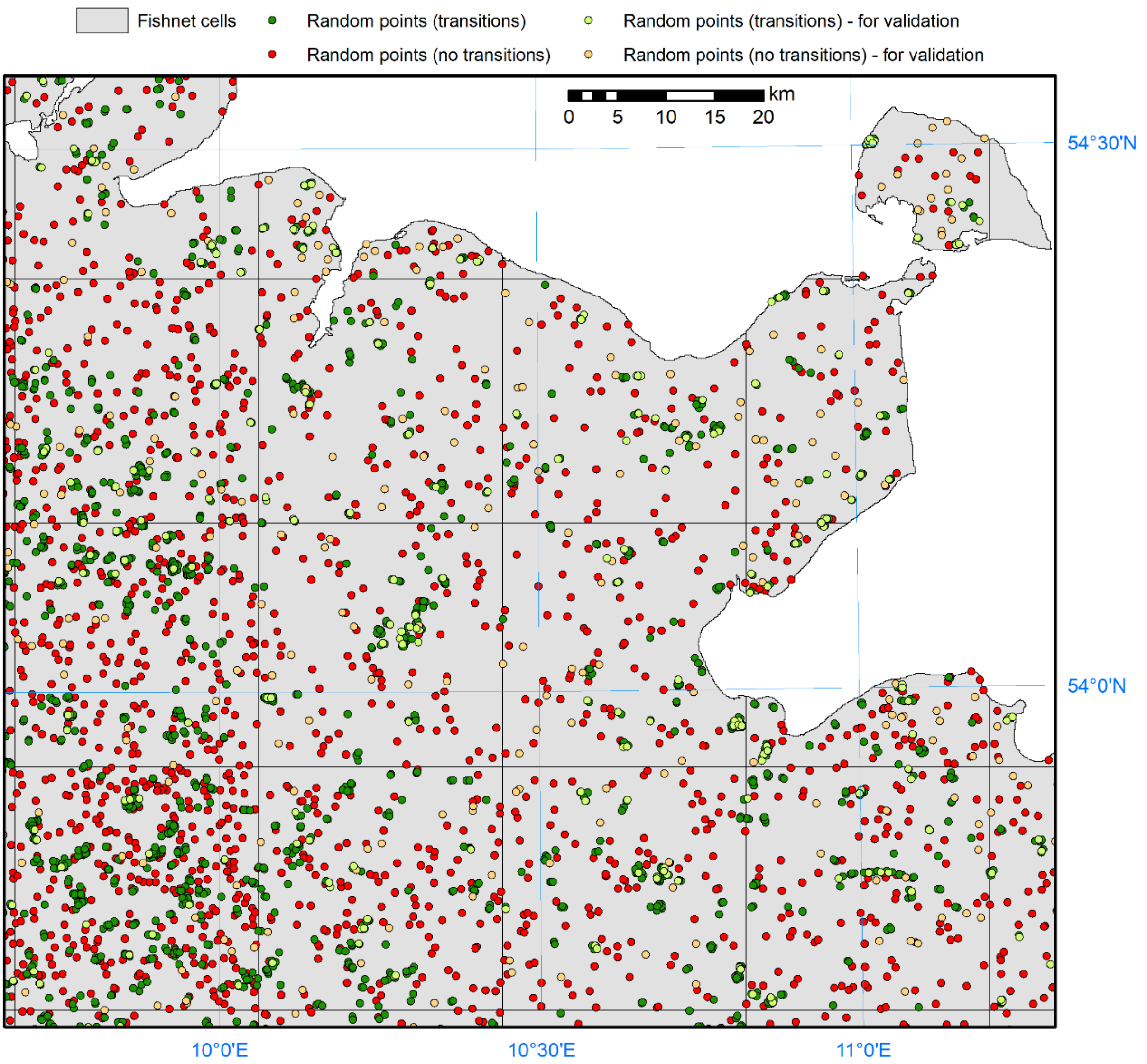

Supplementary Figure S7. Example of sample locations generated for a fragment of northern Germany.

Supplementary Figure S8. Observed population change in Austria

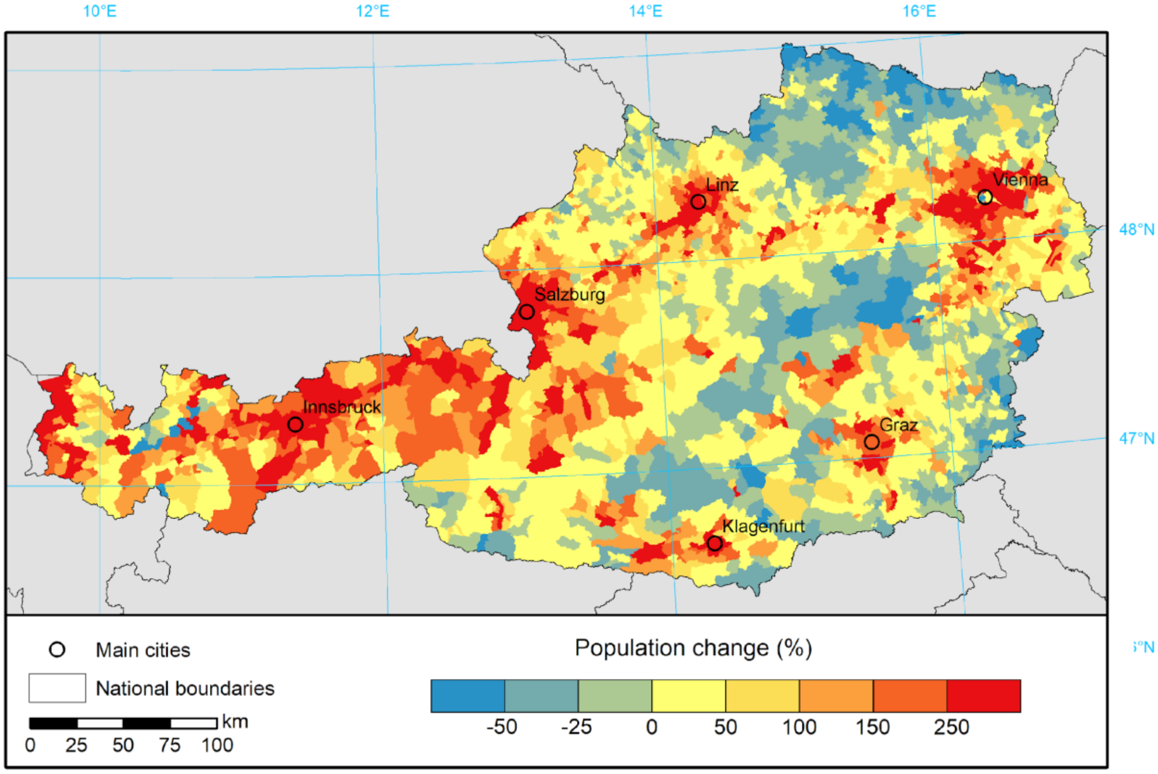

Supplementary Figure S8 Observed population change in Austria by local administrative unit, 1870-2020 (based on Statistik Austria 2022).

Supplementary Figure S9. Drivers of exposure in Europe

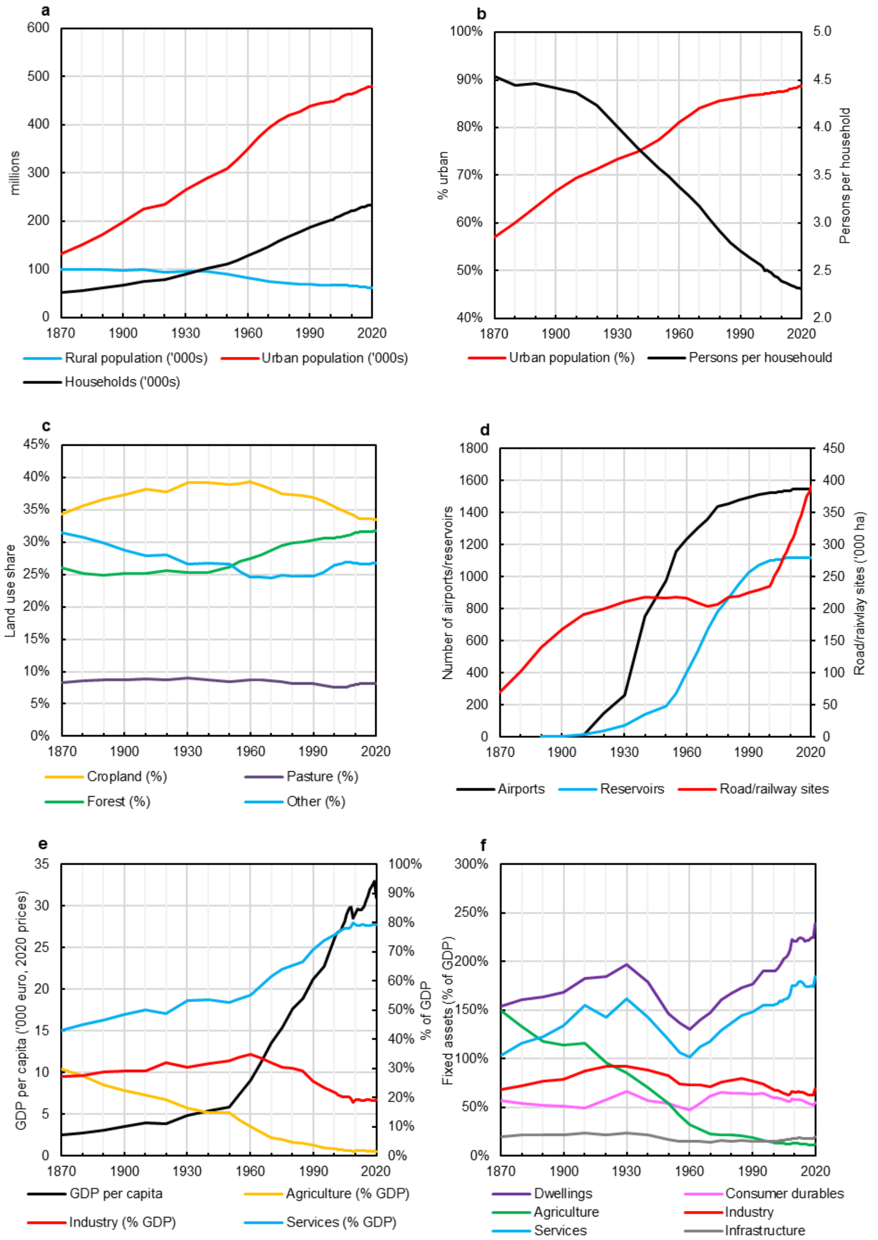

Supplementary Figure S9. Drivers of exposure in Europe, aggregated for the whole study area, 1870-2020. Data on the number of airports and reservoirs are presented in the same temporal resolution as the other drivers.

Supplementary Figure S10. Exposure to coastal floods, 1870-2020

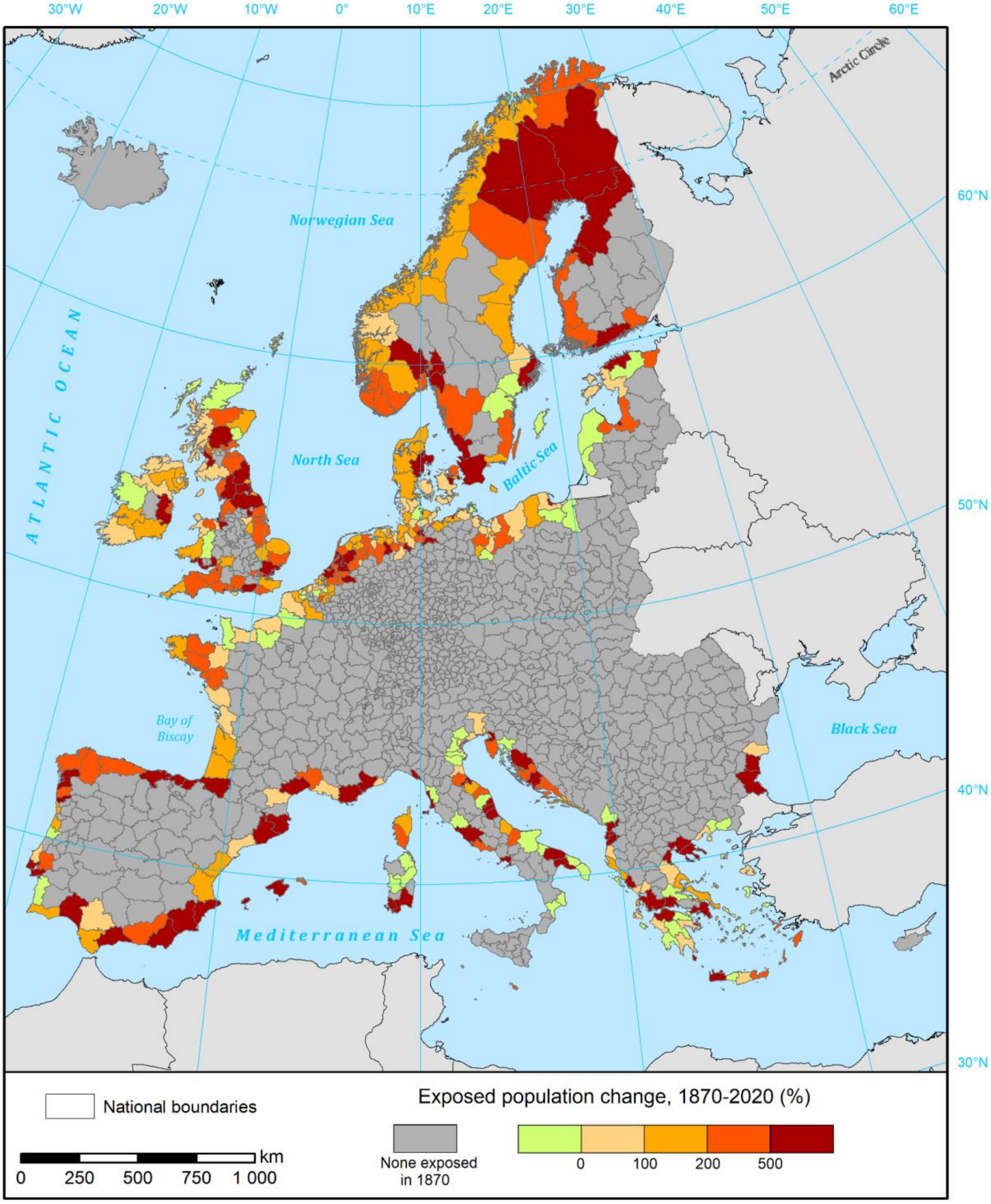

Supplementary Figure S10. Change in the number of population within 100-year coastal flood zones (Paprotny et al. 2019), 1870-2020, aggregated from 100 m resolution to NUTS3 regions.

Supplementary Figure S11. Exposure to floods for selected flood events

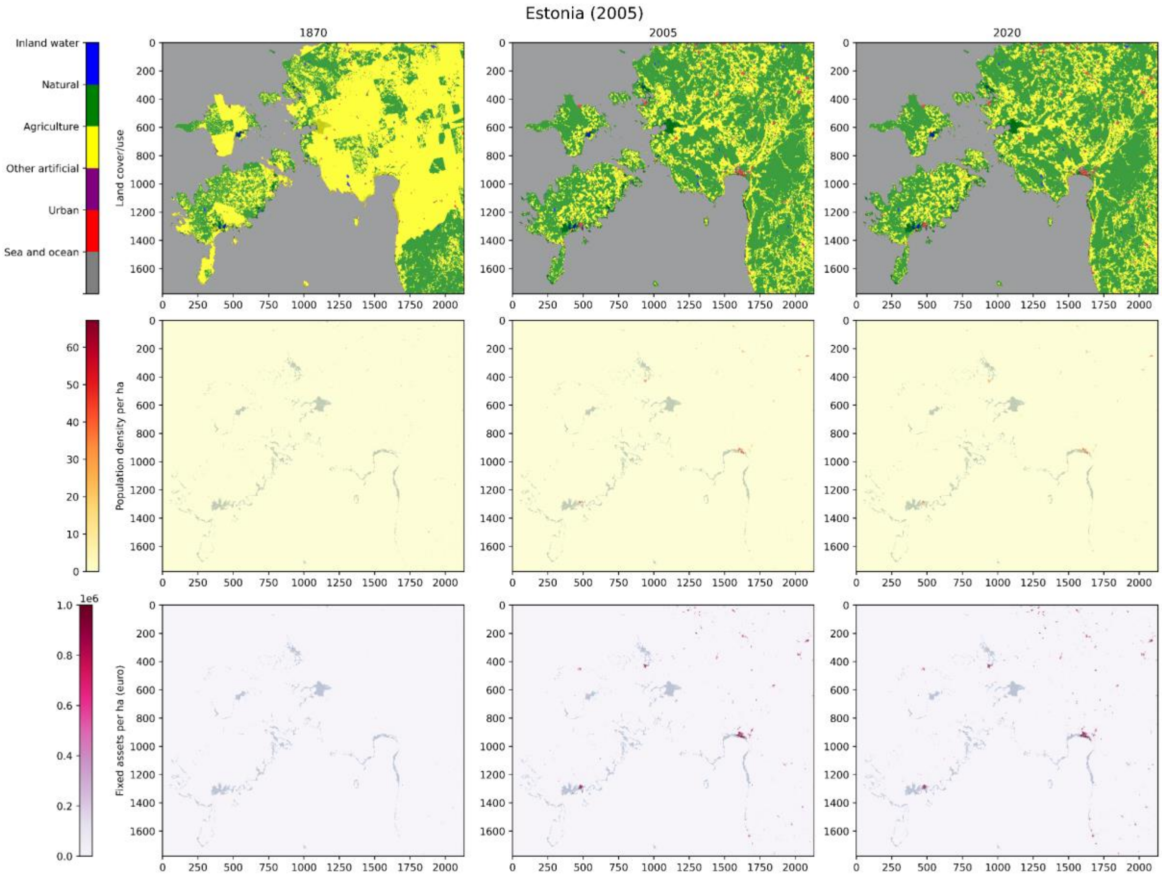

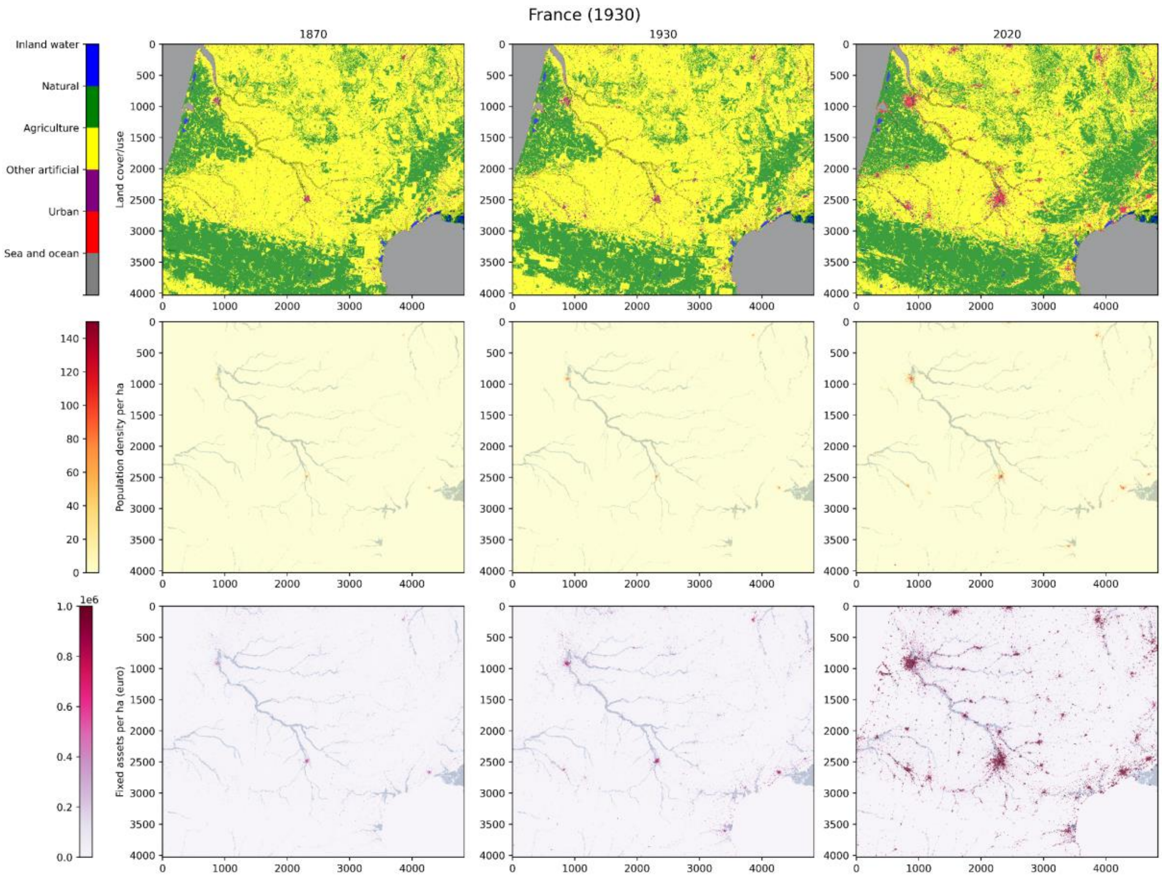

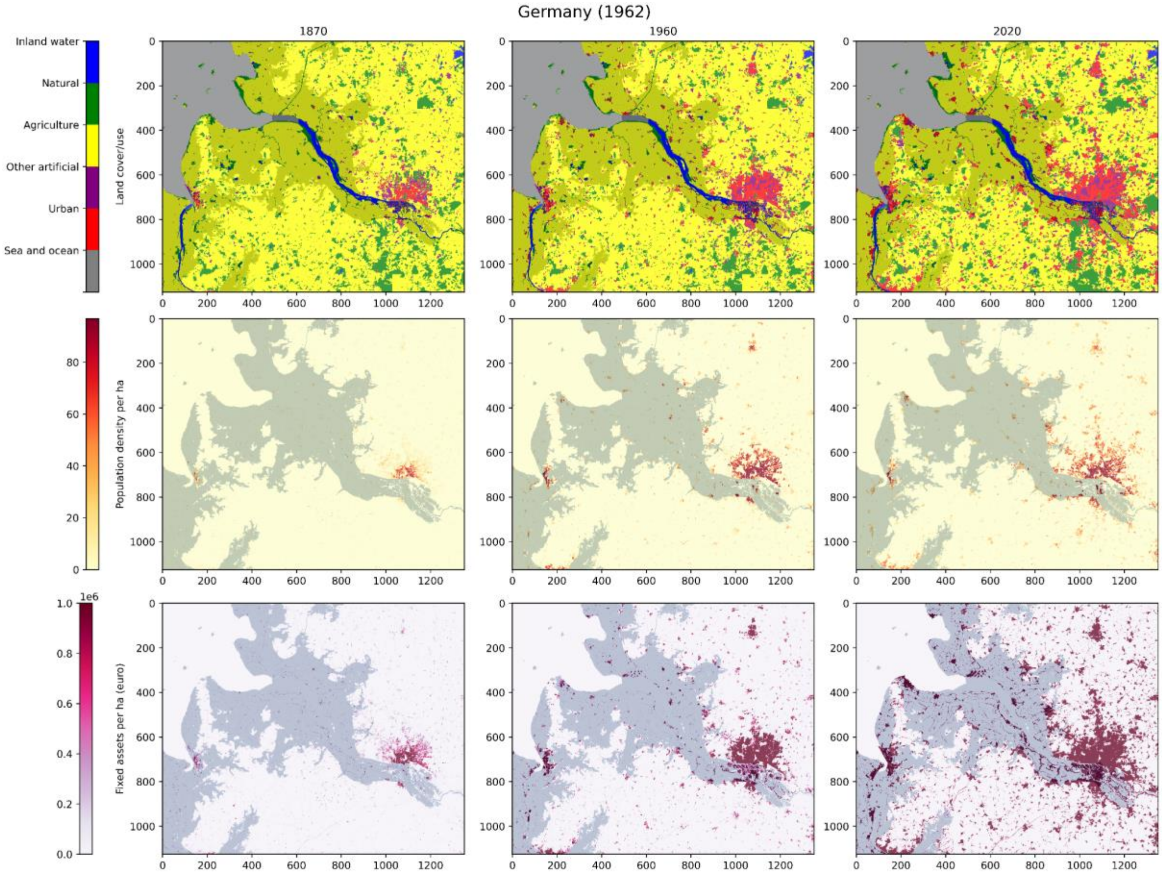

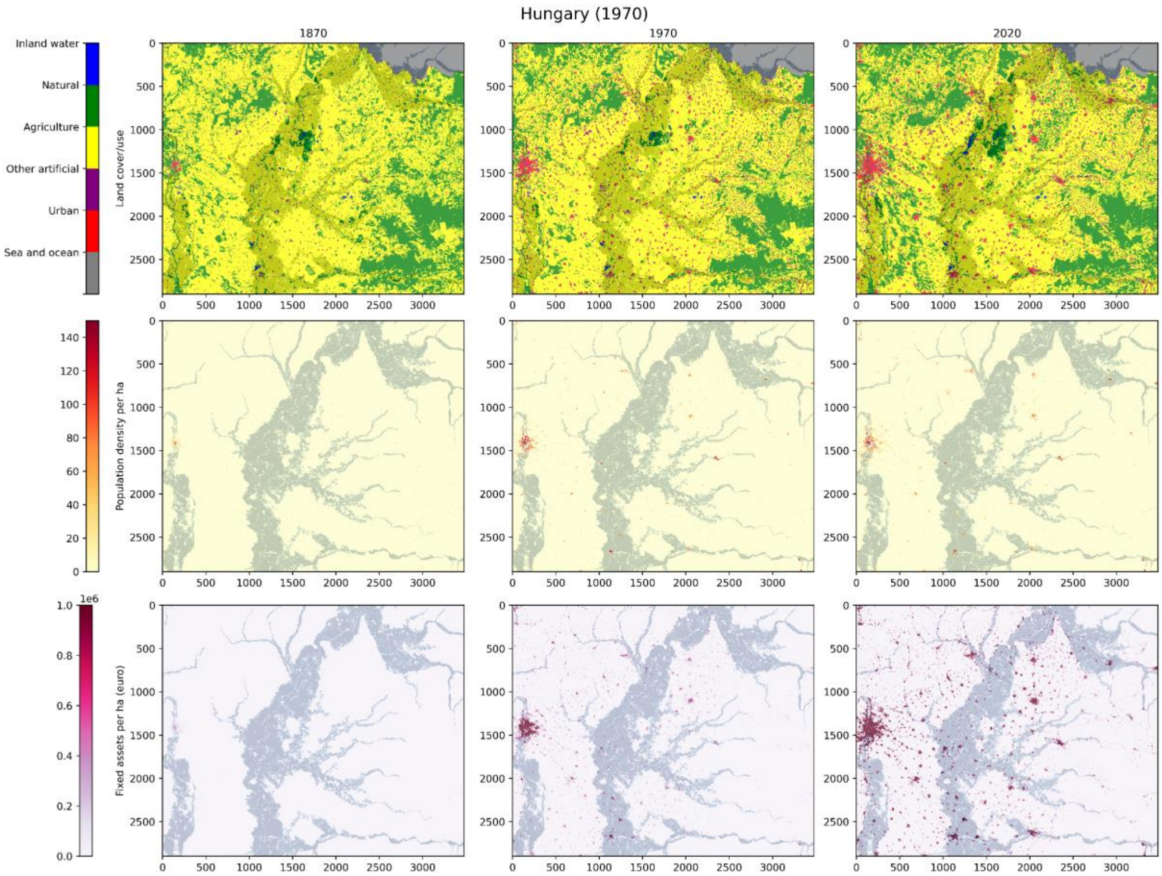

Supplementary Figure S11. Exposure in the vicinity of floods described in the paper, in 1870, timestep nearest to the year of the event and 2020. River or coastal flood hazard zone is shown in the background.

Supplementary Table S3. Input and output files

Supplementary Table S3. List of files of HANZE v2.0 model. XXXX = timestep (year). Sections refer to the main text.

File	Format	Variables / contents
Output		
CLC_XXXX	8-bit GeoTIFF	Land cover/use type, 44 classes according to Corine Land Cover
Pop_XXXX	16-bit GeoTIFF	Total population per grid cell (in persons)
GDP_XXXX	32-bit GeoTIFF	Gross domestic product (GDP) per grid cell per year (euro in constant 2020 prices)
FA_XXXX	32-bit GeoTIFF	Wealth per grid cell (euro in constant 2020 prices)
Imp_XXXX	8-bit GeoTIFF	Soil sealing degree (%)
Input		
Region_database_population_lu	Excel file	Input land use/cover and population data (2.3)
Region_database_economy	Excel file	Input and auxiliary economic data (2.3)
CLC_base_HANZE2	8-bit GeoTIFF	Baseline land cover/use type, 44 classes according to Corine Land Cover (2.2.1)
Population_100m	16-bit GeoTIFF	Total baseline (disaggregated) population per 100 m grid cell (in persons) (2.2.2)
IMD2012_extent_adjusted	8-bit GeoTIFF	Soil sealing degree in % (2.2.1)
NUTS2010_final_100m	Shapefile	NUTS3 (version 2010) region definitions (2.2.3)
NUTS2010_100m_c	8-bit GeoTIFF	NUTS3 region definitions (numerical value from vector file attribute table) (2.2.3)
gras200a_yld_LAEA2	16-bit GeoTIFF	Agro-climatic potential yield for grass (2.4.10)
ylHr0_whe_LAEA2	16-bit GeoTIFF	Output density for wheat (2.4.10)
Airports_year_v2	8-bit GeoTIFF	Airports by year of construction (2.4.4)
Slope_per_mille_int_masked	16-bit GeoTIFF	Slope (per mille) from EU-DEM (2.4.10)
BN_to_urban	16-bit GeoTIFF	Probability map of transition from non-urban to urban after the baseline year (2.4.10)
BN_to_crop	16-bit GeoTIFF	Probability map of transition from non-cropland to cropland after the baseline year (2.4.10)
BN_to_past	16-bit GeoTIFF	Probability map of transition from non-pasture to pasture after the baseline year (2.4.10)
BN_from_crop	16-bit GeoTIFF	Probability map of transition from cropland to non-cropland after the baseline year (2.4.10)

BN_from_past	16-bit GeoTIFF	Probability map of transition from pasture to non-pasture after the baseline year (2.4.10)
BN_to_crop_p	16-bit GeoTIFF	Probability map of transition from non-cropland to cropland before the baseline year (2.4.10)
BN_to_past_p	16-bit GeoTIFF	Probability map of transition from non-pasture to pasture before the baseline year (2.4.10)
BN_from_crop_p	16-bit GeoTIFF	Probability map of transition from cropland to non-cropland before the baseline year (2.4.10)
BN_from_past_p	16-bit GeoTIFF	Probability map of transition from pasture to non-pasture before the baseline year (2.4.10)
ESM2012_street_ext_adj	8-bit GeoTIFF	Surface covered by roads and streets (%) from European Settlement Map 2012 (2.2.2/2.5)
Industry_centroids_int	32-bit GeoTIFF	Distance from centroids of industrial CLC patches in meters (2.4.6)
NL_polders	16-bit GeoTIFF	Year of construction of Dutch polders (2.4.1)
CLC_141_142_selected_v2	32-bit GeoTIFF	Green urban areas and sport facilities than are adjacent to selected artificial surfaces (2.4.9)
CLC2012_urban_d_int	32-bit GeoTIFF	Euclidean distance from centroids of urban CLC 2012 patches (2.4.2)
Clusters2011_high_density_d_int	32-bit GeoTIFF	Euclidean distance from centroids of high-density population clusters (2.4.2)
KernelDensityPop1km_int	32-bit GeoTIFF	Kernel population density with 10-km radius (2.4.1)
UN_agglomerations_d_int	32-bit GeoTIFF	Euclidean distance from centres of large agglomerations and capital cities (2.4.2)
UrbanAudit2018_d_int	32-bit GeoTIFF	Euclidean distance from centroids of cities in Urban Atlas 2018 (2.4.2)
VirtualLAU_PD_int_new	32-bit GeoTIFF	Population density of “virtual” LAUs (2.4.1)
LAU_data	CSV	Population data (1961-2011) per LAU (2.4.1)

Preprocessing data (for reproduction of certain inputs)		
Pure_Population_CLC_cells	CSV	GEOSTAT population 1 km grid cells covered with a single CLC class (2.2.2)
Population_thresholds	CSV	Thresholds for population disaggregation (2.2.2)
ESM2012_buildings	8-bit GeoTIFF	Surface covered by buildings (%) from European Settlement Map 2012 (2.2.2)
GEOSTAT_extent_adjusted	8-bit GeoTIFF	GEOSTAT 1 km population grid (2.2.2)

ESM_GEOSTAT_statistics	CSV	Average population per surface covered by buildings (%) (2.2.2)
ESM_Street_GEOSTAT_statistics	CSV	Average population per surface covered by roads and streets (%) (2.2.2)
IMP_GEOSTAT_statistics	CSV	Average population per surface covered by impervious surfaces (%) (2.2.2)
CLC_changes_sample_data	CSV	CLC land-use transition samples used to train the BN land-use model (2.4.10)
CLC_changes_nosample_data	CSV	CLC land-use non-transition samples used to train the BN land-use model (2.4.10)
BN_sample_data	NumPy file	Processed CLC land-use transition and non-transition samples used to train the BN land-use model (2.4.10)
Validation and analysis data		
LAU2_Austria_pop	Shapefile	Population of Austria by municipality, 1870-2020, for validation (2.6.2)
BN_sample_data_validation	NumPy file	CLC land-use transition and non-transition samples used to validate the BN land-use model (2.6.3)
RAIN_coastalmap_100y	8-bit GeoTIFF	Coastal flood hazard map, 100-year return period (2.6.4)
JRC_flood_mask_100	8-bit GeoTIFF	River flood hazard map, 100-year return period (2.6.4)
Flood_events_v1.0_list	Excel file	Data on damaging floods, 1870-2016, from HANZE v1.0 (2.6.4)

Supplementary references

Clark, C.: Urban Population Densities. Journal of the Royal Statistical Society: Series A, 114(4), 490–496, 1951.

Clark, C.: Population Growth and Land Use. Macmillan, London, 1967.

Copernicus Land Monitoring Service: Pan-European, http://land.copernicus.eu/pan-european/, last accessed 6 May 2022.

Eurostat: GISCO - the Geographic Information System of the COmmission, https://ec.europa.eu/eurostat/web/gisco/overview. Last accessed 21 October 2021.

FAO: Global Agro-Ecological Zoning version 4 (GAEZ v4), https://gaez-data-portal-hqfao.hub.arcgis.com/. Last accessed 25 November 2021.

Gløersen, E. and Lüer, C.: Population data collection for European local administrative units from 1960 onwards - final report. Spatial Foresight GmbH, Luxembourg, 17 pp., 2013 [data available at Eurostat, http://ec.europa.eu/eurostat/web/nuts/local-administrative-units]

Hourihan, K.: Urban Population Density Patterns and Change in Ireland, 1901-1979. The Economic and Social Review, 13(2), 125–147, 1982.

Natural Earth: 1:10m Cultural Vectors, https://www.naturalearthdata.com/downloads/10m-cultural-vectors/, last accessed 8 September 2022.

Paprotny, D., Morales Nápoles, O., Vousdoukas, M. I., Jonkman, S. N., and Nikulin, G.: Accuracy of pan-European coastal flood mapping, J. Flood Risk Manag., 12(2), e12459, doi:10.1111/jfr3.12459, 2019.

Republic of North Macedonia State Statistical Office: https://www.stat.gov.mk/Default_en.aspx. Last accessed 30 October 2021.

Statistical Office of the Republic of Serbia: https://www.stat.gov.rs/en-us/. Last accessed 2 November 2021.

Statistik Austria: http://www.statistik.at/, last accessed 15 February 2022.